NANO LETTERS

Letter

pubs.acs.org/NanoLett

# Magnetogenetic Control of Protein Gradients Inside Living Cells with High Spatial and Temporal Resolution

Fred Etoc,[†] Chiara Vicario,[†] Domenik Lisse,[†,‡] Jean-Michel Siaugue,[§] Jacob Piehler,[‡] Mathieu Coppey,[†] and Maxime Dahan*[,†]

[†]Laboratoire Physico-Chimie, Institut Curie, CNRS UMR168, Paris-Science Lettres, Université Pierre et Marie Curie-Paris 6, 75005 Paris, France

[‡]Department of Biology, University of Osnabrück, 49076 Osnabrück, Germany

[§]Sorbonne Universités, UPMC Univ Paris 06, UMR 8234, PHENIX, F-75005 Paris, France

Supporting Information

**ABSTRACT:** Tools for controlling the spatial organization of proteins are a major prerequisite for deciphering mechanisms governing the dynamic architecture of living cells. Here, we have developed a generic approach for inducing and maintaining protein gradients inside living cells by means of biofunctionalized magnetic nanoparticles (MNPs). For this purpose, we tailored the size and surface properties of MNPs in order to ensure unhindered mobility in the cytosol. These MNPs with a core diameter below 50 nm could be rapidly relocalized in living cells by exploiting biased diffusion at weak magnetic forces in the femto-Newton range. In combination with MNP surface functionalization for specific in situ capturing of target proteins as well as efficient delivery into the cytosplasm, we here present a comprehensive technology for controlling intracellular protein gradients with a temporal resolution of a few tens of seconds.

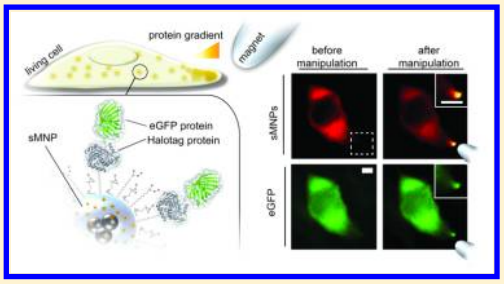


**KEYWORDS:** *Magnetogenetics, nanoparticles, cell signaling, nanomagnetism, intracellular diffusion, protein manipulation*

The spatiotemporal regulation of protein distribution and activity plays a key role in the establishment and maintenance of many cellular functions.[1,2] In past years, several approaches have been developed for exploring protein function by direct manipulation of their activity pattern at a subcellular scale. Photoactivatable reagents and optogenetic approaches have emerged as powerful tools for the local control of protein activity inside living cells.[3] Yet, despite many advantageous properties, light-based activation techniques also present several limitations. In particular, maintaining a well-controlled spatial signaling pattern over extended time periods remains challenging due to diffusional spreading of photoactivated molecules.[4,5] Moreover, optogenetic techniques require expressing genetically modified constructs that can be delicate in vivo and represent, for instance, an obstacle for their future use in cell therapies using human cells.

In this context, magnetic nanoparticles (MNPs) constitute promising tools and offer an alternative to light-based techniques. Functional MNPs can act as defined and controllable nanoplatforms, amenable to noninvasive manipulation inside living cells. MNPs have long been used to investigate the cell response to mechanical perturbations.[6,7] They have also emerged as efficient actuators to remotely trigger cellular signaling, by inducing membrane receptor clustering[8,9] or by activating temperature-sensitive channels[10] (see review in ref 11). More recently, functionalized MNPs manipulated with magnetic forces were used to create and propagate signaling asymmetries within confined bioreactors containing *Xenopus* egg extract.[12−14] In a concomitant study, we established the principles of magnetogenetic manipulation inside living cells.[15] Our strategy relied on functionalized 500 nm MNP which, once microinjected into the cytoplasm, captured genetically modified target proteins of interest (such as RhoGTPases or GEF molecules), and thereby in situ self-assembled into signaling nanoplatforms. Once brought to the plasma membrane using magnetic forces, MNPs locally triggered the activity of the Rac signaling pathway and induced the formation of local actin remodeling and membrane protrusion. Overall this study demonstrated the feasibility of intracellular magnetic manipulation for remote control of cellular signaling.

Yet, a limitation of the approach described above for the control of spatial patterns of activity in living cells was the need to use MNPs with 500 nm diameter. First, MNPs in this size range were difficult to deliver into the cytoplasm by microinjection as they tended to clog pipettes at high concentration and were not compatible with other delivery strategies. As a result, high dilutions of MNPs were employed, which limited us to the injection of a relatively low number of MNPs per cell (5−10 at most). Second, the motion of the 500 nm MNPs was strongly constrained by intracellular obstacles,

**Received:** March 3, 2015
**Revised:** April 15, 2015
**Published:** April 21, 2015





DOI: 10.1021/acs.nanolett.5b00851
*Nano Lett.* 2015, 15, 3487−3494

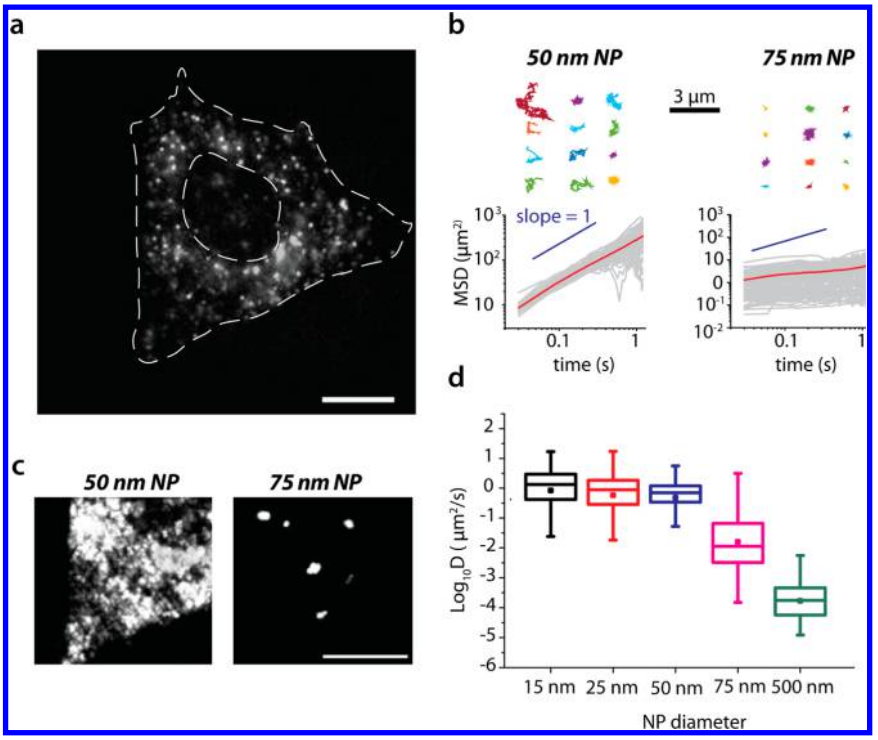


**Figure 1.** NP diffusion in the cytoplasm as a function of their diameter. (a) Epifluorescence image (acquisition time: 50 ms) of fluorescent latex NPs (50 nm in diameter) microinjected in the cytoplasm of a HeLa cell. Single NPs can be resolved. (b) Single trajectory analysis. Top: Examples of NPs intracellular trajectories. Left: 50 nm NPs. Right: 75 nm NPs. Bottom left: MSDs of the 50% fastest 50 nm NPs. Bottom right: MSDs of all the recorded 75 nm NP trajectories. (c) Maximum intensity projection of 300 frames of a movie recorded after injection of 50 nm NPs (left) and 75 nm NPs (right). (d) Box plot representation of the diffusion coefficients obtained for intracellular latex NPs of different sizes. Median (line) and mean (square) of each distribution are indicated.

presumably the cytoskeletal meshwork and the internal membrane network of the endoplasmic reticulum. Thus, magnetic manipulation required forces in the order of 30 pN and nonphysiological conditions such as serum starvation in which the cytoplasmic elasticity was reduced. Under these conditions, it still took several minutes to move the MNPs across the cytoplasm, which represents a low temporal resolution compared to the time scale of the endogeneous Rho-GTPase cycles of activity[16] and many other cell signaling events. Moreover, intracellular gradients of active proteins, as required for many spatially regulated processes,[2] could not be recapitulated with few 500 nm MNPs, which usually clustered at the cell periphery and created punctual signaling perturbations. In a subsequent study, we used 100 nm nonbiofunctionalized magneto-fluorescent core–shell supernanoparticles and found that they could be displaced with forces of ∼1 pN inside cells but still required several minutes to be brought to the membrane.[17]

In the present work, we aimed at advancing magnetogenetic tools inside cells by using much smaller functionalized MNPs in order to enable rapid and facilitated control of intracellular protein gradients with minimum mechanical effects on cellular homeostasis. We show that for MNPs with a hydrodynamic diameter below ∼50 nm, a threshold determined by the viscoelastic properties of the cytoplasm, MNPs exhibit Brownian motion inside the cell. In this regime, weak forces in the femto-Newton range are sufficient to bias MNPs motion and create within a few tens of seconds graded distributions within living cells that have a tunable spatial extension and are fully reversible. Importantly, such small MNPs can be internalized into cells via routes other than microinjection, which makes our method scalable and technically less challenging. Finally, we demonstrate that these MNPs can be functionalized in order to create ectopically graded distributions of proteins within cells. Overall, these developments advance magnetogenetics as a generic tool for unraveling how directional information, encoded under the form of intracellular activity gradients, is detected and processed at the single cell level during key processes such as polarization, migration, or division.

A major challenge that must be overcome when decreasing MNP size is the strong reduction of the magnetic force that can be applied, because the magnetic response approximately scales with the nanoparticle (NP) volume. Yet, the ability of moving intracellular MNPs also depends on the viscoelastic properties of the cytoplasm at the scale of the NP hydrodynamic diameter. In particular, previous work has demonstrated the poro-elastic nature of the cytoplasm in which a solid meshwork composed of the cytoskeleton and the various organelles is immersed in a fluid of low viscosity.[18] We thus expected that there is a critical length scale above which an elastic behavior is dominant and under which the cytoplasm is essentially a viscous medium. To evaluate this critical parameter, we used a standard passive microrheology assay[19] and recorded the trajectories of individual rhodamine-doped latex NPs injected in the cytoplasm of HeLa cells (Figure 1a). We performed these experiments for NPs with diameters of 15, 25, 50, 75, and 500 nm.

After microinjection, latex NPs were homogeneously distributed within the cytoplasm and the majority of these particles remained freely diffusing and stable over extended time periods (Figure 1a and Supporting Information movie S1).



DOI: 10.1021/acs.nanolett.5b00851
*Nano Lett.* 2015, 15, 3487–3494

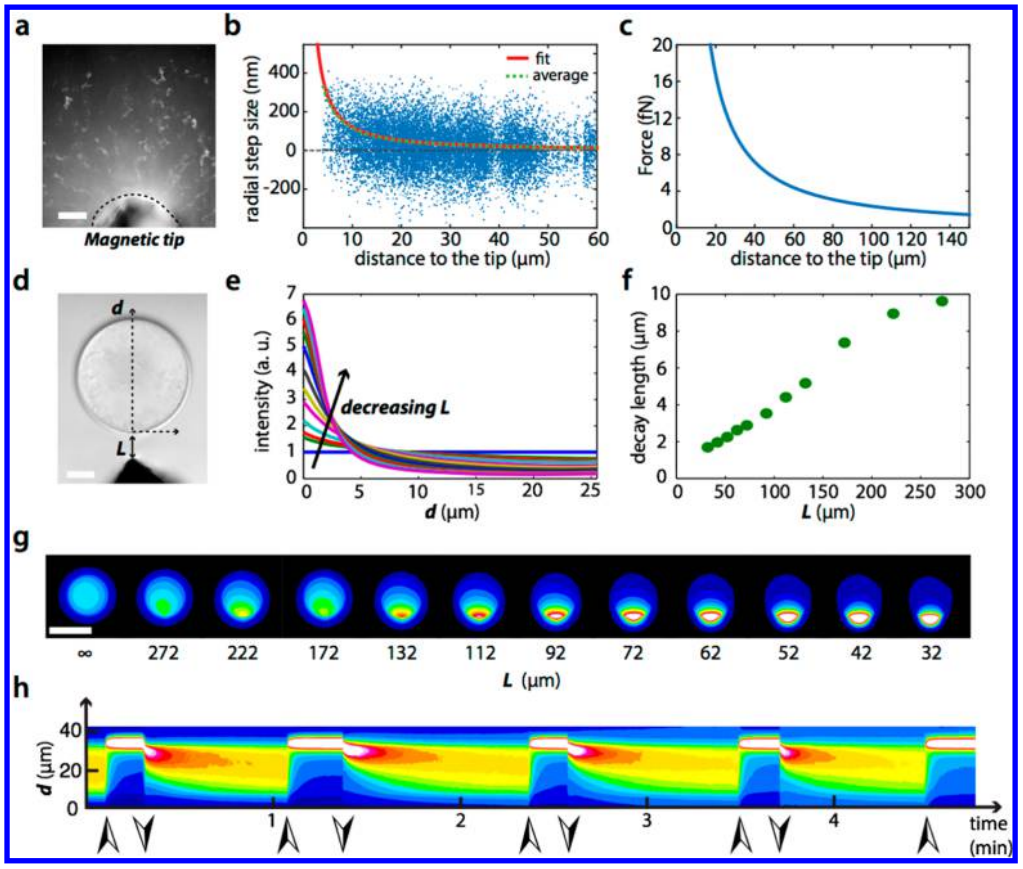


**Figure 2.** In vitro characterization of sMNPs magnetic response. (a) Maximum intensity projection of a movie acquired for the force calibration (Supporting Information movie S3): sMNPs are placed at low concentration in a viscous medium (glycerol/water, 70:30 w/w) and imaged while attracted toward the magnet. (b) Distribution of the sMNPs step sizes in the magnet direction as a function of the distance to the tip. Green dashed line: running average of the data set. Red line: adjustment with a power law fit. (c) Force applied to a single sMNP as a function to the distance to the tip. (d) Droplet assay: A water-in-oil droplet filled with sMNPs is created by microinjection. The magnetic tip is placed at a distance $L$ away from the droplet. Concentrations profiles of sMNPs are analyzed as a function of $d$, position within the droplet. (e) sMNPs' concentration profiles. Each curve represents a different value of $L$. Each curve is corrected for the droplet geometry by dividing by the homogeneous profile inside the droplet in absence of the magnetic tip. (f) Decay length of the sMNP concentration profile as a function of $L$. (g) Images of the sMNP distribution within the droplets for different values of $L$. (h) Kymograph of the sMNP distribution at the droplet equator while the magnetic tip is repeatedly placed at the droplet vicinity and removed (Supporting Information movie S4).

As shown by the maximum intensity projection of the associated movies (Figure 1c and Supporting Information movie S2) and a few illustrative individual trajectories (Figure 1b), NPs with diameter under 50 nm were diffusing in the cytoplasm over long distances while NPs of 75 nm (and above) exhibited a strongly confined motion. Diffusion properties were quantitatively assessed by computing for each trajectory its mean-square displacement (MSD) and diffusion coefficient. The 15, 25, and 50 nm nanoparticles had relatively similar behavior (Figure 1d), with distributions of diffusion coefficients peaking around 1 $\mu m^2/s$. In contrast, for nanoparticles with diameter 75 nm and above, the median diffusion coefficient dropped by several order of magnitudes and was around 0.01 $\mu m^2/s$ for 75 nm NPs and 0.0001 $\mu m^2/s$ for 500 nm NPs (Figure 1d). Within the poro-elastic paradigm, the strong nonlinearity in the cytoplasmic elasticity as NP size increases can be linked to the diameter of the NP exceeding the effective pore size of the cytoplasm. Consistently, when individual MSD curves were extracted we noticed that the motion of 75 nm NP was subdiffusive (Figure 1b, bottom), suggesting elastic trapping, while for most 50 nm (and below) NPs the MSDs scaled linearly with time, indicative of standard Brownian diffusion (Figure 1b, bottom). Taken as a whole, our results point to a sharp transition in the viscoelastic properties of the cytoplasm. Below a size threshold around 50 nm, there is a viscous regime: NP diffusion is mostly Brownian within a medium that is ~10 times more viscous than water. Above this threshold, we encounter an elastic regime, where NPs are confined within the solid phase of the cytoplasm. These observations are qualitatively consistent with prior measurements using recovery after photobleaching for fluorescent dextran molecules with varying lengths.[20]

On the basis of our rheological observations, we hypothesized that MNPs small enough to fall into the viscous regime could be manipulated inside living cells, even though they were subjected to weak magnetic forces. In the following, we used core−shell MNPs[21] composed of a core of superparamagnetic maghemite nanoparticles embedded in a silica matrix enriched with rhodamine molecules for fluorescence imaging. Moreover, their surface was functionalized with short PEG chains (seven ethylene glycol units in average) in order to ensure proper surface passivation and to minimize nonspecific interactions, as well as with amino groups to allow further functionalization. The mean hydrodynamic diameter of these MNPs (hereafter designed as small MNPS, sMNPs) was ~40 nm and their saturation magnetization $3 \times 10^5$ A/m.[21]



DOI: 10.1021/acs.nanolett.5b00851
*Nano Lett.* 2015, 15, 3487−3494

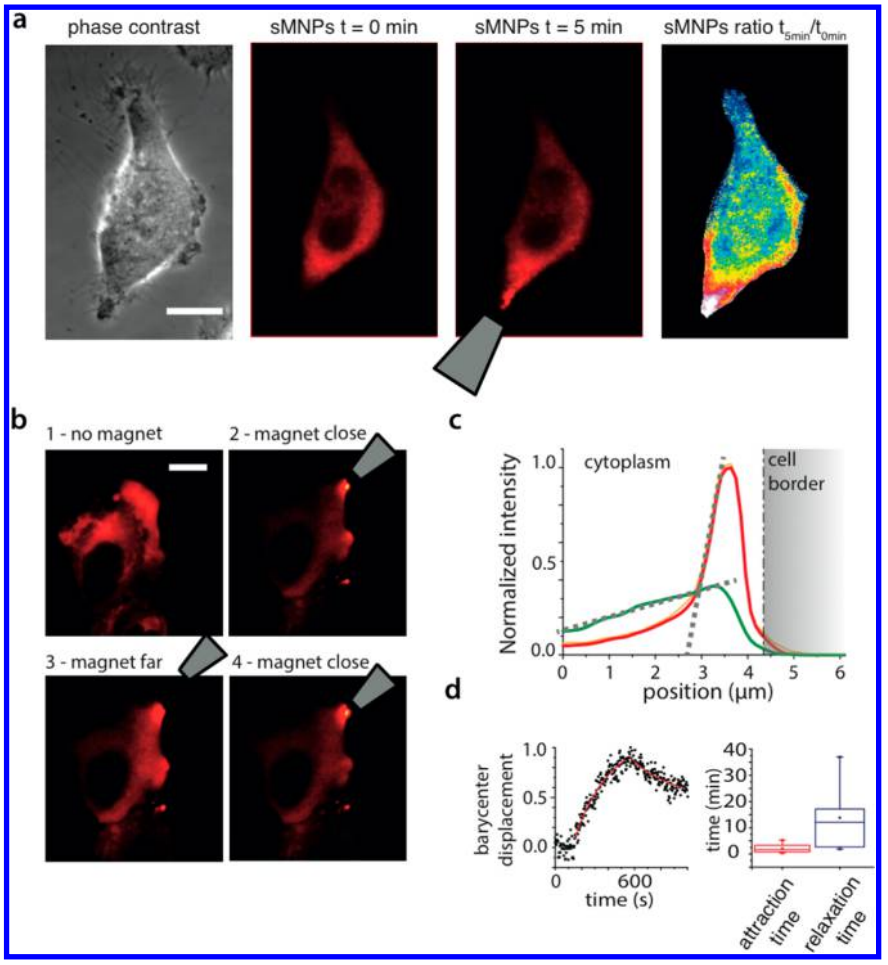


**Figure 3.** Magnetic manipulation of sMNPs inside living cells. (a) Application of magnetic forces with the magnetic tip results in the attraction of sMNPs at the edge of the cell. Left: phase contrast image. Middle-left: sMNP distribution before magnet application. Middle-right: sMNP distribution after magnet application. Right: Ratio of the two middle images in pseudocolor. Scale bar: 10 $\mu$m. (b) Epifluorescence images of sMNP microinjected into a HeLa cell (top left). The magnetic tip is approached near (~2 $\mu$m) the cell periphery (top right), then moved ~10 $\mu$m away (bottom left), and near the cell again (bottom right). (c) Quantification of the steady-state particle profiles established in the cell shown in panel b, when the magnetic tip is placed close to the cell (green curve), and away (red curve). (d) Attraction and relaxation kinetics of sMNPs (left) and characteristic times for particle attraction (red) and relaxation (blue) (right).

In order to apply forces to the sMNPs, we used homemade magnetic tips with an approximately parabolic shape, prepared as described previously.[15] The common procedure to determine the force generated by a magnetic tip on MNPs consists in tracking the ballistic motion of the nanoparticles within a medium of calibrated viscosity and determining their instantaneous velocity as they are attracted by the magnetic tip. By means of the Stokes law, it yields a calibration curve of the applied force as a function of the distance to the tip. In our case, for sMNP subjected to magnetic gradients on the order of $10^3$–$10^4$ T/m, magnetic forces are in the femto-Newton range, too weak to produce clear ballistic MNP trajectories toward the magnetic tip. Rather, the motion of sMNP appears as a biased diffusion toward the magnetic tip, resulting from the superposition of a Brownian motion with a magnetic drift, both of which producing sMNP translocations of equivalent amplitudes between two consecutive frames (Figure 2a and Supporting Information movie S3).

To analyze trajectories of individual sMNP, we measured for each individual translocation the radial step size, defined as the projected distance in the direction of the magnet (positive values pointing toward the magnet, Figure 2b). As expected, far from the magnetic tip, radial step sizes are distributed symmetrically around zero, consistent with a purely Brownian motion. Closer to the magnetic tip, radial step sizes get shifted toward more positive values reflecting the influence of the magnetic drag. A running average of these data yielded a curve that could be satisfyingly approximated by a power law (Figure 2b). We used the power law adjustment to compute the force to distance curve thanks to the Stokes relationship $F = 6\pi\eta r v$, where $\eta$ is the dynamic viscosity, $r$ is the sMNP radius, and $v$ is the sMNP velocity (computed as the mean radial step size divided by the acquisition time). On the basis of this calibration, it follows that for sMNPs within 20 and 150 $\mu$m from the tip, the magnetic forces vary between 15 and 1 fN (Figure 2c). Our results are also consistent with measurements obtained on larger MNPs (500 nm).[15] Note that a power law spatial dependence of the magnetic field gradient slightly differs from the dependence predicted for a magnetic parabolic tip,[7] which we attributed to the tilt of the tip with respect to the coverslip and to deviations from an ideal parabolic shape.

Next, we investigated whether forces in the femto-Newton range could reproducibly generate graded distributions of sMNPs in a viscous medium. In order to mimic the physical



DOI: 10.1021/acs.nanolett.5b00851
*Nano Lett.* 2015, 15, 3487–3494

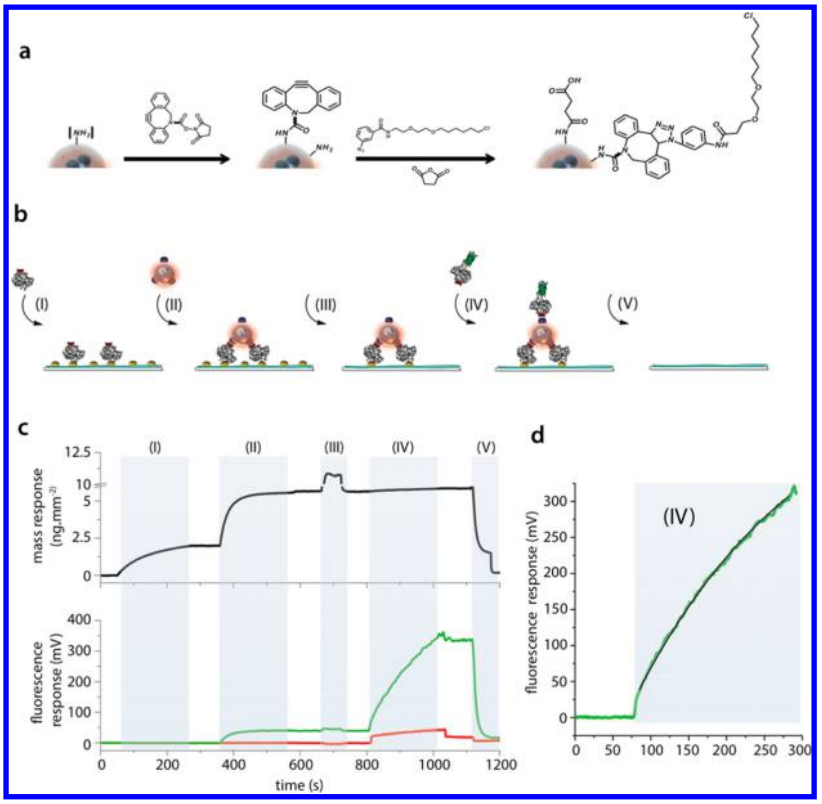


**Figure 4.** sMNP surface functionalization and functional characterization in vitro. (a) Coupling of DBCO and followed by click reaction with an optimized azido-HTL derivative to form clickHTL-functionalized sMNPs. In the final step, excess surface amines were converted into carboxyl groups by reaction with succinic anhydride. (b) Probing the reaction kinetics of the HaloTag with $^{clickHTL}$sMNPs by TIRF/RIfs detection. Immobilization of HaloTag-H12 (I), binding of 5 nM $^{clickHTL}$sMNPs to immobilized HaloTag-H12 (II), wash with EDTA to remove free Ni(II) ions bound to Tris-NTA (III), binding of 1 $\mu$M HaloTag-mEGFP-H6 (HT-eGFP-H6) to immobilized $^{clickHTL}$sMNPs (IV and IVa), and surface regeneration by washing with HCL. (c) (Top) Label-free detection by RIf; (bottom) green fluorescence detection (eGFP signal) with some bleed-through from the rhodamine in the sMNP shell (green curve). As a negative control, binding of 1 $\mu$M HT-eGFP-H6 in the absence of immobilized sMNPs is shown (red curve). (d) Binding curve of HT-eGFP-H6 and fit of a monoexponential association model.

confinement in living cells, we used an in vitro model system made of viscous droplets inside oil (diameter around 50 $\mu$m) formed by injecting a nanomolar aqueous solution of sMNPs in a mixture of mineral oil and surfactant (L-$\alpha$-phosphatidylcholine) on top of a PDMS substrate. In the presence of the magnetic tip, a sharp gradient of sMNPs rapidly formed in the droplet with an extension dependent on the magnet position (Figure 2d–g). In principle, application of a constant force $F$ to a confined population of Brownian diffusing magnetic nanoparticle should lead to an exponential distribution with a decay length $\lambda = kT/F$, with $k$ being the Boltzmann constant and $T$ is the temperature. In our case, the magnetic force $F$ is not constant over the droplet but decreases with the distance to the tip (Figure 2c). However, variation of the magnetic force through the droplet extension was small enough that sMNPs distributions could be adjusted by exponential curves (Figure 2e). As expected, the distribution decay length decreased when reducing the distance between the droplet and the tip, which is equivalent to increasing the applied force (Figure 2f,h). We were able to create exponential distributions with adjustable decay lengths between 2 and 10 $\mu$m. Importantly, we verified the reversibility of the gradient formation by dynamically monitoring sMNP distribution while approaching and removing the tip. A kymograph of the fluorescence, recorded along the droplet midplane during multiple cycles, indicated that the gradient of sMNPs is completely reversible with no sign of aggregation (Figure 2h and Supporting Information movie S4). In the aqueous environment of the droplet, steady-state was reached in about a second, and the relaxation time needed to homogeneously redisperse the sMNPs was about 20 s (Figure 2h). Taken together, our experiments confirmed the ability to generate reversible, tunable, graded profiles of nanoparticles in a confined, viscous medium that mimic the cytoplasm of a living cell.

In order to translate our results into live cell applications, we carefully tuned sMNP surface characteristics. Indeed, the intracellular diffusion and manipulation of nanoparticles strongly depend on their interaction with proteins, organelles and intracellular compartments.[22] We therefore investigated the stability of sMNPs in the cytoplasm of living cells as a function of their surface charge. To this end, sMNPs were microinjected into HeLa cells and their colloidal stability was investigated over 30 min. We initially used PEG and amine-coated sMNPs (exhibiting a $\zeta$-potential of +20 mV at pH 7.4), in which case the nanoparticles were immediately localized at the plasma membrane, likely due to electrostatic interactions with negatively charged lipids (Supporting Information Figure S1). To overcome this issue, surface exposed amines were converted to carboxyl groups by reaction with succinic anhydride (Supporting Information Figure S1). At a $\zeta$-potential = −2 mV, sMNPs were trapped within intracellular compartments 30 min after microinjection. Further stabilization of colloidal properties inside cells were achieved by fully converting surface exposed amines to carboxyl groups ($\zeta$-potential = −20 mV), in


DOI: 10.1021/acs.nanolett.5b00851
*Nano Lett.* 2015, 15, 3487–3494

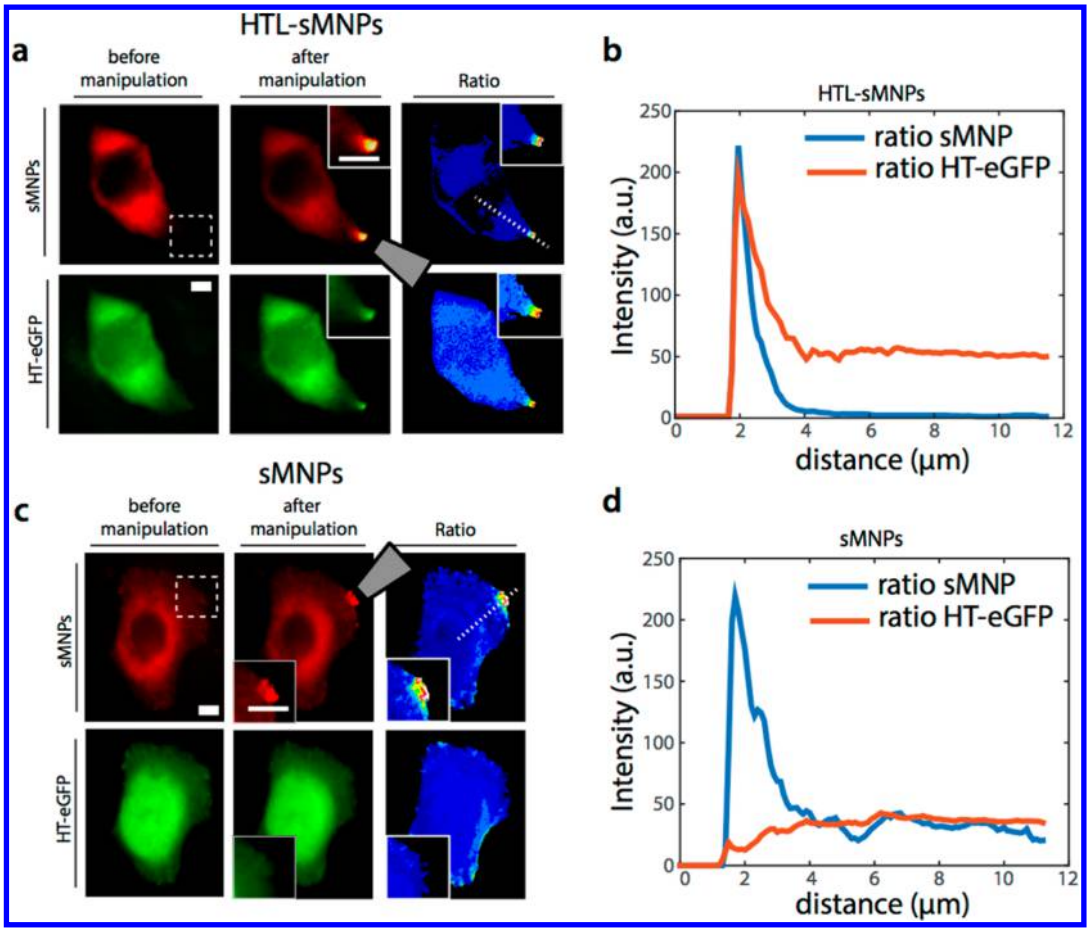


**Figure 5.** Spatiotemporal control of protein gradients inside living cells. (a) HeLa cell transfected with HT-eGFP (bottom, GFP fluorescence in green) and injected with click-HTL-functionalized sMNPs (top, Rhodamine fluorescence in red). On the right column are ratiometric images of the corresponding channels (image after manipulation divided by the image and before manipulation). Scale bar 10 $\mu$m. (b) Intensity profiles of the ratiometric images in panel a. (c) Control experiment using nonfunctional sMNP. Same organization as panel a. (d) Intensity profiles of the ratiometric images in panel c.

which case the particles remained freely diffusing during the observation time (Supporting Information Figure S1).

With stabilized carboxyl-coated sMNPs at hand, we investigated whether we could reproducibly induce a tunable gradient of nanoparticles inside living cells. To this end, HeLa cells were loaded with sMNPs by using either microinjection, osmotic lysis of pynocitic vesicles[23,24] or a bead loading technique.[25] All these approaches resulted into a homogeneous dispersion of freely diffusing sMNPs within the cytoplasm (Figure 3a Supporting Information movie S5). When bringing the magnetic tip close to the plasma membrane, the nanoparticles were attracted to the cell edge (Figure 3a and Supporting Information movie S5), creating sharp and graded sMNPs distributions. We explored the kinetics of attraction/relaxation of the sMNP by tracking individual sMNP positions after force application and removal. Analysis of the barycenter of sMNPs localization within individual cells showed typical time for magnetic attraction on the order of 1 min and relaxation on the order of 10 min (Figure 3d and Supporting Information movie S6). These distributions were stable in time over durations of at least tens of minutes (Supporting Information movie S7) and reversible.

In order to explore the tunability of the sMNP concentration profile within living cells, we placed the tip ~2 $\mu$m away from the cell membrane, yielding an exponential distribution with decay length of 0.8 $\mu$m (Figure 3b,c). Subsequently, the tip was moved back by about 10 $\mu$m. At steady state, the gradient was much weaker with a characteristic decay length of 14 $\mu$m. Remarkably, when we brought the tip back to its original position the distribution was directly comparable to the initial one (gradient decay length of 0.8 $\mu$m). This observation showed that tunable concentration profiles can be reproducibly and rapidly achieved inside living cells by adjusting the applied force. The distributions inside cells had an extension ranging between 1 and 15 $\mu$m, comparable to what had been obtained in vitro (Figure 2d–h). Yet, the time-scales of gradient establishment and dispersion inside cells are about ten times longer than the one observed in vitro within aqueous droplets. This observation qualitatively matches the results obtained earlier by single particle tracking showing that NP diffusion, below 50 nm in diameter, is mostly Brownian in a medium ten times more viscous than water. We thus concluded that concentration gradients of sMNPs inside living cells can be reversibly established upon application of femto-Newton forces, based on a mechanism of biased random walk within the fluid phase of the cytoplasm.

For rendering sMNP biofunctional, we engineered their surface properties to enable specific capturing of target proteins within the cytoplasm of living cells. For this purpose, sMNPs were functionalized with a HaloTag-ligand and delivered into



DOI: 10.1021/acs.nanolett.5b00851
*Nano Lett.* 2015, 15, 3487–3494

cells expressing the protein of interest fused to the HaloTag.[15,26] This strategy was chosen because it allows self-assembly of biofunctional sMNPs inside living cells. sMNPs exhibited a great quantity of amine groups (~5000 per particle) on the surface offering versatile means for chemical modification of surface properties. In our case, amine groups were used to couple an engineered HaloTag ligand obtained by click chemistry (clickHTL), which provides an improved rate constant of the reaction with the HaloTag.[22] To this end, the nanoparticles were reacted with a commercially available dibenzocyclooctyne (DBCO)-like derivate prior to click reaction and surface carboxylation (Figure 4a).

Different DBCO concentrations were titrated in order to maximize protein binding on the nanoparticle surface (Supporting Information Figure S2). In the following, sMNPs were reacted with an excess of 1500 DBCO molecules per particle yielding a degree of functionalization of around 150 DBCO molecules covalently bound to the particle surface. This degree of functionalization was thought to be sufficient to saturate the particle surface with HaloTag fusion proteins as estimated based on previous experiments.[26] Furthermore, the reaction kinetics of clickHTL functionalized nanoparticles was evaluated in vitro. To this end, we probed by simultaneous total internal reflection fluorescence spectroscopy (TIRFS) and reflectance interference (TIRFS-Rlf) detection[27] the reaction of immobilized nanoparticles with purified HaloTag fused to mEGFP and a hexahistidine-tag (HaloTag-eGFP-H6) (Figure 4b). $^{clickHTL}$sMNPs were immobilized via a purified HaloTag fused to a dodecahistidine-tag (HaloTag-H12) on a PEG brush functionalized with Tris-NTA. Binding of HaloTag-eGFP-H6 to immobilized $^{clickHTL}$sMNPs was characterized after removing excess Ni(II) ions bound to Tris-NTA. The resulting binding curve indicated a reaction rate constant $5.0 \times 10^3$ $M^{-1}$ $s^{-1}$, which is in good agreement with the reaction rate constant observed for binding of HaloTag-eGFP to the negative charged surface of polystyrene nanoparticles functionalized with clickHTL.[26]

Finally, we aimed to demonstrate the potential of sMNP to control the spatial distribution of target proteins inside living cells. For the proof of principle, we injected clickHTL-functionalized sMNPs into COS7 cells overexpressing mEGFP fused to the HaloTag (HT-eGFP, Figure 5a). We next positioned the magnetic tip close to the cell edge and monitored the fluorescence in the mEGFP (green) and rhodamine (red) channels. Strikingly, the green and red fluorescence signals simultaneous increased at the proximity of the tip and were colocalized (Figure 5a). As shown by the ratio of the sMNPs and HT-eGFP distributions before and after magnetic manipulation (Figure 5a,b), both distributions were superimposed in the closer region to the magnet, demonstrating a net magnetic displacement of the GFP proteins by the sMNPs. Further inside the cell, ratiometric signal from sMNPs and the HT-eGFP were nonoverlapping, reflecting the presence of a population of untargeted HT-eGFP with a cytoplasmic localization that remains independent of the magnetic force due to the excess of unbound HT-eGFP. To ensure that the magnetic manipulation of eGFP protein was indeed induced by specific binding of the HT-eGFP to the sMNPs, we monitored HT-eGFP distributions in the presence of a magnetic gradient when sMNPs not functionalized with clickHTL were used (Figure 5c,d). In these control experiments, we observed a gradient of sMNPs but no change in eGFP distribution. Thus, $^{clickHTL}$sMNPs and HT-eGFP signals are not correlated due to experimental bias, for example, by volume effect due to pressure application on the membrane by the sMNPs or by nonspecific interactions but because of specific capturing of HT-eGFP molecules by $^{clickHTL}$sMNPs. Overall, these experiments establish that we succeeded to engineer sMNPs suitable for specifically recruiting and spatially redistribute target proteins inside cells by magnetic forces.

In conclusion, we achieved spatiotemporal control of the intracellular distribution of proteins captured to sub-50 nm sMNPs. Although intracellular manipulation of small MNPs has been shown previously,[28,29] it relied on the displacement of endosomes loaded with multiple MNPs. This did not permit the targeting of cytosolic components and the versatile control of their signaling activities. Furthermore, it often required several hours to move the nanoparticle-loaded endosomes across the cytoplasm.[28] A breakthrough in our experiments was to use MNPs with a diameter below 50 nm, which behaved as Brownian particles in the cytoplasm. While the applied forces were in the femto-Newton range, which is much weaker than, for example, the pico-Newton forces exerted by a single molecular motor,[30] the sMNP could be readily manipulated with response times on the order of a few tens of seconds, which are significantly shorter than the ones (several minutes) observed in the case of large 100−500 nm diameter MNPs. Moreover, at the cell periphery, we could establish and control the spatial profile of MNP distributions with a gradient steepness depending on the magnetic field strength and varying between 1 and 15 $\mu$m. Next to sMNP size, an engineered surface functionalization of sMNPs was essential for magnetic manipulation. By using negative surface charges to ensure prolonged stability in the cytoplasm in combination with the HaloTag-system for efficient capturing of target proteins in situ, minimum increase in sMNP diameter was achieved that enabled unhindered manipulation after biofunctionalization. Proof-of-concept experiments with HT-eGFP as a model target protein clearly demonstrated the ability to achieve a graded concentration profile inside the cell. Importantly, sMNPs do not require microinjection for internalization, and efficient delivery by standard internalization protocols can be readily achieved. Remarkably, while we chose to manipulate overexpressed eGFP proteins, similar experiments could be performed with sMNPs biofunctionalized in vitro prior to internalization, allowing manipulation of genetically nonmodified cells. Thus, our study lays the foundations for the magnetic or magnetogenetic manipulation of virtually any intracellular proteins or biomolecules such as DNA, RNA, or small organic ligands. In our experiments, we used a rudimentary magnetic tip. Yet, by means of microfabrication techniques, it is possible to design magnetic substrates that optimize the characteristics of the magnetic gradients. Furthermore, combining microfabricated substrates and micropatterning should allow parallel manipulation of MNPs in thousands of individual cells.[29] Thus, we envision that our approach paves the way toward novel assays for probing in a noninvasive manner the cellular response to spatially controlled signaling perturbations and for remote actuation of intracellular signaling pathways.

## ■ ASSOCIATED CONTENT

### Supporting Information

Synthesis scheme of clickHTL, nanoparticle functionalization protocols, optimization of intracellular sMNP stability, cell culture, microinjection and microscopy. Supplementary movies: intracellular diffusion of 50 nm NP and 70 nm NPs, in vitro and



DOI: 10.1021/acs.nanolett.5b00851
Nano Lett. 2015, 15, 3487−3494

in vivo manipulation of sMNPs. This material is available free of charge via the Internet at http://pubs.acs.org.

## AUTHOR INFORMATION


### Corresponding Author

*E-mail: maxime.dahan@curie.fr.

### Present Address

(F.E.) Center for Studies in Physics and Biology and Laboratory of Molecular Vertebrate Embryology, The Rockefeller University, New York.


### Author Contributions

F.E., C.V., and D.L. performed the experiments and analyzed the data. J.M.S. provided the nanoparticles. D.L. and J.P. provided reagents. F.E., D.L., J.P., M.C., and M. D. conceived the project. The manuscript was written through contributions of all authors. All authors have given approval to the final version of the manuscript.

F.E., C.V., and D.L. contributed equally.

### Notes

The authors declare no competing financial interest.

## ACKNOWLEDGMENTS

M.D. acknowledges financial support from French National Research Agency (ANR) Paris-Science-Lettres Program (ANR-10-IDEX-0001-02 PSL), Labex CelTisPhyBio (No. ANR-10-LBX-0038), the Human Frontier Science Program (Grant RGP0005/2007).

## ABBREVIATIONS

MNP, magnetic nanoparticle; eGFP, monomeric enhanced green fluorescent protein

## REFERENCES


(1) Kholodenko, B. N.; Hancock, J. F.; Kolch, W. Signalling Ballet in Space and Time. *Nat. Rev. Mol. Cell Biol.* **2010**, *11*, 414−426.

(2) Kinkhabwala, A.; Bastiaens, P. I. H. Spatial Aspects of Intracellular Information Processing. *Curr. Opin. Genet. Dev.* **2010**, *20*, 31−40.

(3) Gautier, A.; Gauron, C.; Volovitch, M.; Bensimon, D.; Jullien, L.; Vriz, S. How to Control Proteins with Light in Living Systems. *Nat. Chem. Biol.* **2014**, *10*, 533−541.

(4) Wu, Y. I.; Frey, D.; Lungu, O. I.; Jaehrig, A.; Schlichting, I.; Kuhlman, B.; Hahn, K. M. A Genetically Encoded Photoactivatable Rac Controls the Motility of Living Cells. *Nature* **2009**, *461*, 104−108.

(5) Levskaya, A.; Weiner, O. D.; Lim, W. a; Voigt, C. a. Spatiotemporal Control of Cell Signalling Using a Light-Switchable Protein Interaction. *Nature* **2009**, *461*, 997−1001.

(6) Wilhelm, C. Out-of-Equilibrium Microrheology inside Living Cells. *Phys. Rev. Lett.* **2008**, *101*, 028101.

(7) De Vries, A. H. B.; Krenn, B. E.; van Driel, R.; Kanger, J. S. Micro Magnetic Tweezers for Nanomanipulation inside Live Cells. *Biophys. J.* **2005**, *88*, 2137−2144.

(8) Mannix, R. J.; Kumar, S.; Cassiola, F.; Montoya-Zavala, M.; Feinstein, E.; Prentiss, M.; Ingber, D. E. Nanomagnetic Actuation of Receptor-Mediated Signal Transduction. *Nat. Nanotechnol.* **2008**, *3*, 36−40.

(9) Cho, M. H.; Lee, E. J.; Son, M.; Lee, J.-H.; Yoo, D.; Kim, J.; Park, S. W.; Shin, J.-S.; Cheon, J. A Magnetic Switch for the Control of Cell Death Signalling in in Vitro and in Vivo Systems. *Nat. Mater.* **2012**, *11*, 1038−1043.

(10) Huang, H.; Delikanli, S.; Zeng, H.; Ferkey, D. M.; Pralle, A. Remote Control of Ion Channels and Neurons through Magnetic-Field Heating of Nanoparticles. *Nat. Nanotechnol.* **2010**, *5*, 602−606.

(11) Bonnemay, L.; Celine, H.; Gueroui, Z. Remote Control of Signaling Pathways Using Magnetic Nanoparticles. *Wiley Interdiscip. Rev.: Nanomed. Nanobiotechnol.* **2014**.

(12) Hoffmann, C.; Mazari, E.; Lallet, S.; Le Borgne, R.; Marchi, V.; Gosse, C.; Gueroui, Z. Spatiotemporal Control of Microtubule Nucleation and Assembly Using Magnetic Nanoparticles. *Nat. Nanotechnol.* **2013**, *8*, 199−205.

(13) Bonnemay, L.; Hostachy, S.; Hoffmann, C.; Gautier, J.; Gueroui, Z. Engineering Spatial Gradients of Signaling Proteins Using Magnetic Nanoparticles. *Nano Lett.* **2013**, *13*, 5147−5152.

(14) Hoffmann, C.; Mazari, E.; Gosse, C.; Bonnemay, L.; Hostachy, S.; Gautier, J.; Gueroui, Z. Magnetic Control of Protein Spatial Patterning to Direct Microtubule Self-Assembly. *ACS Nano* **2013**, *7*, 9647−9654.

(15) Etoc, F.; Lisse, D.; Bellaiche, Y.; Piehler, J.; Coppey, M.; Dahan, M. Subcellular Control of Rac-GTPase Signalling by Magnetogenetic Manipulation inside Living Cells. *Nat. Nanotechnol.* **2013**, *8*, 193−198.

(16) Nalbant, P.; Hodgson, L.; Kraynov, V.; Toutchkine, A.; Hahn, K. M. Activation of Endogenous Cdc42 Visualized in Living Cells. *Science* **2004**, *305*, 1615−1619.

(17) Chen, O.; Riedemann, L.; Etoc, F.; Herrmann, H.; Coppey, M.; Barch, M.; Farrar, C. T.; Zhao, J.; Bruns, O. T.; Wei, H.; et al. Magneto-Fluorescent Core-Shell Supernanoparticles. *Nat. Commun.* **2014**, *5*, 5093.

(18) Moeendarbary, E.; Valon, L.; Fritzsche, M.; Harris, A. R.; Moulding, D. a; Thrasher, A. J.; Stride, E.; Mahadevan, L.; Charras, G. T. The Cytoplasm of Living Cells Behaves as a Poroelastic Material. *Nat. Mater.* **2013**, *12*, 253−261.

(19) Weihs, D.; Mason, T. G.; Teitell, M. a. Bio-Microrheology: A Frontier in Microrheology. *Biophys. J.* **2006**, *91*, 4296−4305.

(20) Verkman, A. S. Solute and Macromolecule Diffusion in Cellular Aqueous Compartments. *Trends Biochem. Sci.* **2002**, *27*, 27−33.

(21) Georgelin, T.; Bombard, S.; Siaugue, J.-M.; Cabuil, V. Nanoparticle-Mediated Delivery of Bleomycin. *Angew. Chem., Int. Ed.* **2010**, *49*, 8897−8901.

(22) Lisse, D.; Richter, C. P.; Drees, C.; Birkholz, O.; You, C.; Rampazzo, E.; Piehler, J. Monofunctional Stealth Nanoparticle for Unbiased Single Molecule Tracking inside Living Cells. *Nano Lett.* **2014**, *14*, 2189−2195.

(23) Okada, C. Y.; Rechsteiner, M. Introduction of Macromolecules into Cultured Mammalian Cells by Osmotic Lysis of Pinocytic Vesicles. *Cell* **1982**, *29*, 33−41.

(24) Pierobon, P.; Achouri, S.; Courty, S.; Dunn, A. R.; Spudich, J. a; Dahan, M.; Cappello, G. Velocity, Processivity, and Individual Steps of Single Myosin V Molecules in Live Cells. *Biophys. J.* **2009**, *96*, 4268−4275.

(25) Mcneil, P. L.; Warder, E. Glass Beads Load Macromolecules into Living Cells. *J. Cell Sci.* **1987**, *88*, 669−678.

(26) Lisse, D.; Wilkens, V.; You, C.; Busch, K.; Piehler, J. Selective Targeting of Fluorescent Nanoparticles to Proteins inside Live Cells. *Angew. Chem., Int. Ed.* **2011**, *50*, 9352−9355.

(27) Gavutis, M.; Lata, S.; Piehler, J. Probing 2-Dimensional Protein-Protein Interactions on Model Membranes. *Nat. Protoc.* **2006**, *1*, 2091−2103.

(28) Gao, J.; Zhang, W.; Huang, P.; Zhang, B.; Zhang, X.; Xu, B. Intracellular Spatial Control of Fluorescent Magnetic Nanoparticles. *J. Am. Chem. Soc.* **2008**, *130*, 3710−3711.

(29) Tseng, P.; Judy, J. W.; Carlo, D. Di. Magnetic Nanoparticle − Mediated Massively Parallel Mechanical Modulation of Single-Cell Behavior. *Nat. Methods* **2012**, *9*, 1113−1119.

(30) Svoboda, K.; Block, S. M.; Boulevard, E. L. Force and Velocity Measured for Single Kinesin Molecules. *Cell* **1994**, *77*, 773−784.




DOI: 10.1021/acs.nanolett.5b00851
*Nano Lett.* 2015, 15, 3487−3494